Acquirement of water-splitting ability and alteration of the charge-separation mechanism in photosynthetic reaction centers

Hiroyuki Tamura[a,b], Keisuke Saito[a,b], and Hiroshi Ishikita[a,b,1]

[a]Department of Applied Chemistry, The University of Tokyo, Tokyo 113-8654, Japan; and [b]Research Center for Advanced Science and Technology, The University of Tokyo, Tokyo 153-8904, Japan

Edited by Paul G. Falkowski, Rutgers University, New Brunswick, NJ, and approved June 2, 2020 (received for review January 16, 2020)

In photosynthetic reaction centers from purple bacteria (PbRC) and the water-oxidizing enzyme, photosystem II (PSII), charge separation occurs along one of the two symmetrical electron-transfer branches. Here we report the microscopic origin of the unidirectional charge separation, fully considering electron–hole interaction, electronic coupling of the pigments, and electrostatic interaction with the polarizable entire protein environments. The electronic coupling between the pair of bacteriochlorophylls is large in PbRC, forming a delocalized excited state with the lowest excitation energy (i.e., the special pair). The charge-separated state in the active branch is stabilized by uncharged polar residues in the transmembrane region and charged residues on the cytochrome c_2 binding surface. In contrast, the accessory chlorophyll in the D1 protein (Chl_{D1}) has the lowest excitation energy in PSII. The charge-separated state involves $Chl_{D1}^{\bullet+}$ and is stabilized predominantly by charged residues near the Mn_4CaO_5 cluster and the proceeding proton-transfer pathway. It seems likely that the acquirement of water-splitting ability makes Chl_{D1} the initial electron donor in PSII.

unidirectional electron transfer | oxygen evolution | P680 | excitation energy transfer | artificial photosynthesis

In photosystem II (PSII), the driving force of water oxidation is provided by light-induced charge separation in the reaction center. In PSII, the reaction center has a pair of chlorophylls, P_{D1}/P_{D2}, accessory chlorophylls, Chl_{D1}/Chl_{D2}, pheophytins, $Pheo_{D1}$/$Pheo_{D2}$, and plastoquinones, Q_A/Q_B, in the heterodimeric D1/D2 protein subunit pairs (Fig. 1) (1). Notably, the crystal structures of PSII and purple bacterial photosynthetic reaction centers (PbRC) show a large structural similarity (2). In PbRC, the reaction center has a pair of bacteriochlorophylls, P_L/P_M, accessory bacteriochlorophylls, B_L/B_M, bacteriopheophytins, H_L/H_M, and ubiquinones (or menaquinones), Q_A/Q_B, in the heterodimeric L/M protein subunit pairs (Fig. 1). P_L and P_M form the electronically coupled special pair [P_LP_M]. Electronic excitation of [P_LP_M] leads to the formation of the charge-separated state, $[P_LP_M]^{\bullet+}B_L^{\bullet-}$, and subsequent electron transfer occurs to Q_B via H_L and Q_A (3). The cationic state $[P_LP_M]^{\bullet+}$ is reduced by electron transfer from an outer protein subunit, cytochrome c_2 (in PbRC from *Rhodobacter sphaeroides* or tetraheme cytochrome in PbRC from *Blastochloris viridis*). In PSII, transfer of excitation energy from the surrounding antenna chlorophylls to the reaction-center chlorophylls (4, 5) leads to the formation of the cationic state $[P_{D1}P_{D2}]^{\bullet+}$, which has a significantly high redox potential (E_m) for one-electron oxidation [>1,100 mV (6–9)] with respect to $[P_LP_M]^{\bullet+}$ [500 mV (10)]. The high E_m makes $[P_{D1}P_{D2}]^{\bullet+}$ abstract electrons from the substrate water molecules at the Mn_4CaO_5 moiety [700 to 800 mV (11)] via redox-active D1-Tyr161 (TyrZ).

In both PbRC and PSII, electron transfer predominantly occurs along the L- and D1-branches, not the M- and D2-branches, irrespective of the pseudo-C_2 symmetry between the two branches (12–14). Because exciton is stabilized by electron–hole Coulomb interaction, charge separation necessitates a sufficient potential offset between electron donor and acceptor cofactors. In PbRC, the energy levels of the charge-separated states were investigated in mutant proteins (15–18). Recent theoretical studies suggested that the redox potential of B_L for one-electron reduction, $E_m(B_L)^{0/\bullet-}$, is significantly higher than $E_m(B_M)^{0/\bullet-}$, which suggests that the $B_L^{\bullet-}$ formation is more stabilized than the $B_M^{\bullet-}$ formation (19). The factors that increase $E_m(B_L)^{0/\bullet-}$ with respect to $E_m(B_M)^{0/\bullet-}$ are 1) the difference in the polarity of the uncharged L/M residue pairs in the hydrophobic transmembrane region [e.g., Phe-L181/Tyr-M210 (19, 20)], 2) acidic residues that provide the binding interface of cytochrome c_2 on the protein surface of subunit M [e.g., Glu-M95 and Asp-M184 (19, 21)], and 3) a cluster of hydrophobic residues that form the carotenoid binding site (19).

In contrast to PbRC, $E_m(Chl_{D1})^{0/\bullet-}$ is lower than $E_m(Chl_{D2})^{0/\bullet-}$ in PSII, which suggests that $Chl_{D1}^{\bullet-}$ is unstable and $[P_{D1}/P_{D2}]^{\bullet+}Chl_{D1}^{\bullet-}$ is not relevant as a charge-separated intermediate (19). This is in line with the proposal that $Chl_{D1}^{\bullet+}Pheo_{D1}^{\bullet-}$ is the charge-separated state in PSII (22–24). The D1/D2 residue pairs that (destabilize $Chl_{D1}^{\bullet-}$ with respect to $Chl_{D2}^{\bullet-}$ and) stabilize $Chl_{D1}^{\bullet+}$ with respect to $Chl_{D2}^{\bullet+}$ are involved in the Mn_4CaO_5 cluster or the proceeding proton transfer pathway (e.g., D1-Asp61/D2-His61, D1-Asp170/D2-Phe169, D1-Asn181/D2-Arg180, and D1-Glu189/D2-Phe188) (19). The absence of the corresponding residues in PbRC implies that the energetic difference between

Significance

In photosynthetic reaction centers from purple bacteria (PbRC) and the water-splitting enzyme, photosystem II (PSII), light-induced electron transfer occurs only in one of the two branches irrespective of the apparent symmetry in the structures. In PSII, the protein components that are involved in the Mn_4CaO_5 cluster or the proceeding proton-transfer pathway facilitate electron transfer along the active branch. In PbRC, most of these components are not conserved and polar residues on the active side facilitate electron transfer. The energy profile suggests that the initial electron donor differs between PbRC and PSII. It seems likely that the acquirement of oxygen-evolving ability alters the protein environment near the accessory chlorophyll and makes it the initial electron donor in PSII.

Author contributions: H.I. designed research; H.T., K.S., and H.I. performed research; H.T., K.S., and H.I. analyzed data; and H.I. wrote the paper.

The authors declare no competing interest.

This article is a PNAS Direct Submission.

This open access article is distributed under Creative Commons Attribution-NonCommercial-NoDerivatives License 4.0 (CC BY-NC-ND).

[1]To whom correspondence may be addressed. Email: hiro@appchem.t.u-tokyo.ac.jp.

This article contains supporting information online at https://www.pnas.org/lookup/suppl/doi:10.1073/pnas.2000895117/-/DCSupplemental.

First published June 29, 2020.

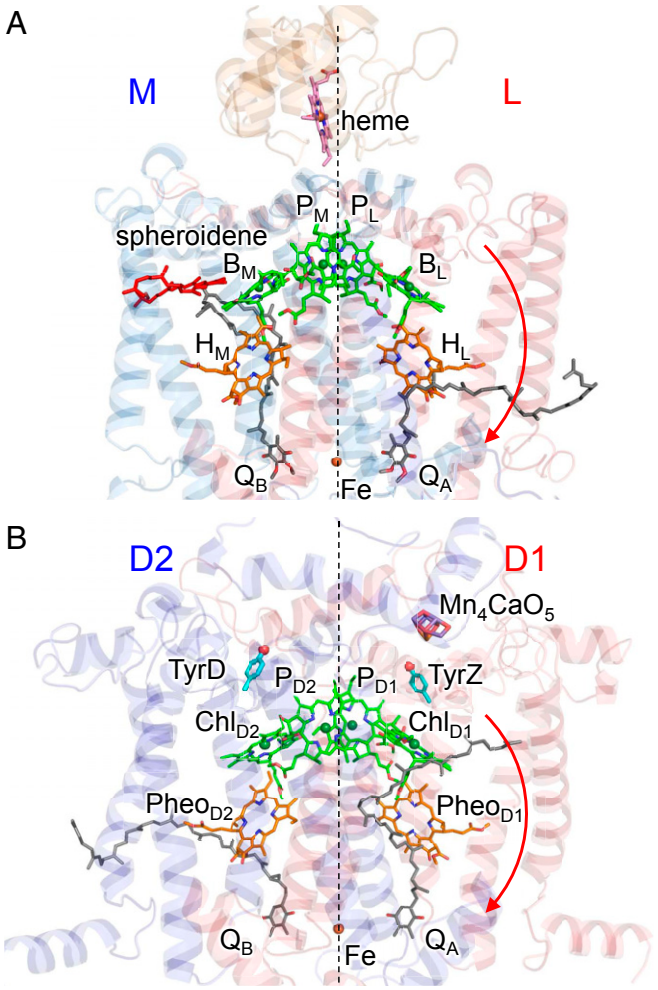

Fig. 1. Electron transfer chains in photosynthetic reaction centers of (*A*) PSII (PDB ID code 3ARC) and (*B*) PbRC from *R. sphaeroides* (PDB ID codes 3I4D and 1L9B). Red arrows indicate electron transfer. Dotted lines indicate pseudo-C_2 axes. Electron-transfer active branches are labeled in red and inactive branches in blue.

B_L/B_M in PbRC and Chl_{D1}/Chl_{D2} in PSII is associated with the presence of the water-splitting components in PSII.

The reported E_m values of cofactors show the energetic difference between the two symmetrical electron transfer branches before light-induced charge separation occurs, that is, the ground state (19). However, the E_m profile also shows that both electron-transfer branches are energetically downhill in PSII (19). This suggests that the unidirectional charge separation cannot be explained solely from the E_m profile, because the charge-separated intermediate states are involved in the electron transfer process. As far as we are aware, the energy levels of the electronically excited states and the subsequent charge-separated states in the two branches and the protein components that facilitate unidirectional electron transfer are not reported for the two reaction centers. It remains thus far unclear why light-induced electron transfer occurs only in one of the two electron transfer branches irrespective of the apparent symmetry in the protein structure. It is also an open question why the charge-separation mechanism is likely to differ between PbRC and PSII, irrespective of the apparent structural similarity (14).

Here we report the energetics of electronically excited states and charge-separated states in PbRC and PSII, using a combined quantum mechanical/molecular mechanical/polarizable continuum model (QM/MM/PCM) approach with density functional theory (DFT) and time-dependent DFT (TDDFT) and considering electron–hole interaction (i.e., exciton binding energy), electronic coupling, and electrostatic interactions with the polarizable, entire protein environments.

Results

Initial Electron Donor $[P_LP_M]$ in PbRC. The excitonic coupling of 27 meV between P_L^* and P_M^* in the PbRC protein environment (Table 1) is sufficiently larger than interaction between the excited state and the protein electrostatic environment [e.g., 10 to 15 meV (25)]. The TDDFT-QM/MM calculations show that the $[P_LP_M]$ pair has the lowest excitation energy among the bacteriochlorophylls (Fig. 2). The formation of the $[P_LP_M]$ pair leads to a decrease of 230 to 270 meV in the excitation energy with respect to the monomeric P_L and P_M bacteriochlorophylls (Fig. 2). The large couplings between other excited states (e.g., 136 meV between P_L^* and $P_L^{\bullet+}P_M^{\bullet-}$; *SI Appendix*, Table S1) also contributes to the decrease in the $[P_LP_M]$ pair excitation energy.

For other factors, electrostatic interactions with the protein environment contribute to a decrease of 70 to 110 meV in the excitation energy of the monomeric P_L and P_M bacteriochlorophylls (Table 2). The larger contribution of the protein electrostatics to P_L^* (109 meV) than P_M^* (70 meV) is due to the presence of the H-bond between P_L and His-L168. Deformations of the chlorin rings induced by interactions with the protein environment (26, 27) contribute to a decrease of 50 meV in the excitation energy of the monomer P_L and P_M bacteriochlorophylls. It seems likely that $[P_LP_M]$ is an electronically coupled special pair, serving as the initial electron donor in PbRC (Fig. 2).

Charge-Separated State $[P_LP_M]^{\bullet+}B_L^{\bullet-}$ in PbRC. When the interaction between electron and hole is considered quantum-chemically in TDDFT-QM/MM/PCM calculations (28), the charge-separated state in the L-branch, $[P_LP_M]^{\bullet+}B_L^{\bullet-}$, is 281 meV more energetically stable than the corresponding charge-separated state in the M-branch, $[P_LP_M]^{\bullet+}B_M^{\bullet-}$ (Fig. 2). The energy difference remains unchanged even when the intramolecular reorganization energy is considered (285 meV) (*SI Appendix*, Fig. S2). In the presence of the intramolecular reorganization energy, charge separation from $[P_LP_M]^*$ to $[P_LP_M]^{\bullet+}B_L^{\bullet-}$ is 55 meV energetically downhill, whereas charge separation from $[P_LP_M]^*$ to $[P_LP_M]^{\bullet+}B_M^{\bullet-}$ is 230 meV uphill.

The energy difference between $[P_LP_M]^{\bullet+}B_L^{\bullet-}$ and $[P_LP_M]^{\bullet+}B_M^{\bullet-}$ is predominantly due to the energy difference between $B_L^{\bullet-}$ and $B_M^{\bullet-}$ (i.e., the difference in the lowest unoccupied molecular orbital [LUMO] energy, which corresponds to the difference in E_m for one-electron reduction) because $[P_LP_M]^{\bullet+}$ can be considered to be equidistant from B_L and B_M (even if the $P_L^{\bullet+}/P_M^{\bullet+}$ population alters slightly, depending on $B_L^{\bullet-}$ and $B_M^{\bullet-}$). The key L/M residue pairs that stabilize $B_L^{\bullet-}$ with respect to $B_M^{\bullet-}$ are summarized in Table 3. In the Tyr-L67/Glu-M95 and Asp-L155/Asp-M184 pairs, Glu-M95 and Asp-M184 provide the binding interface of the electron-donor cytochrome c_2 (21), destabilize the $B_M^{\bullet-}$ formation, and thus decrease $E_m(B_M)$ (Fig. 3*A*) (19). It is characteristic to PbRC that polar, uncharged residues stabilize $B_L^{\bullet-}$ with respect to $B_M^{\bullet-}$. The Phe-L181/Tyr-M210 pair is located near B_M/B_L, and the difference has been suggested to be

Table 1. Electronic and excitonic coupling for the $[P_LP_M]$ bacteriochlorophyll pair in PbRC and the $[P_{D1}P_{D2}]$ chlorophyll pair in PSII in millielectron volts (centimeters^{-1})

	PbRC	PSII
Excitonic coupling	27 (218)	10 (81)
Electronic coupling	114 (919)	13 (105)

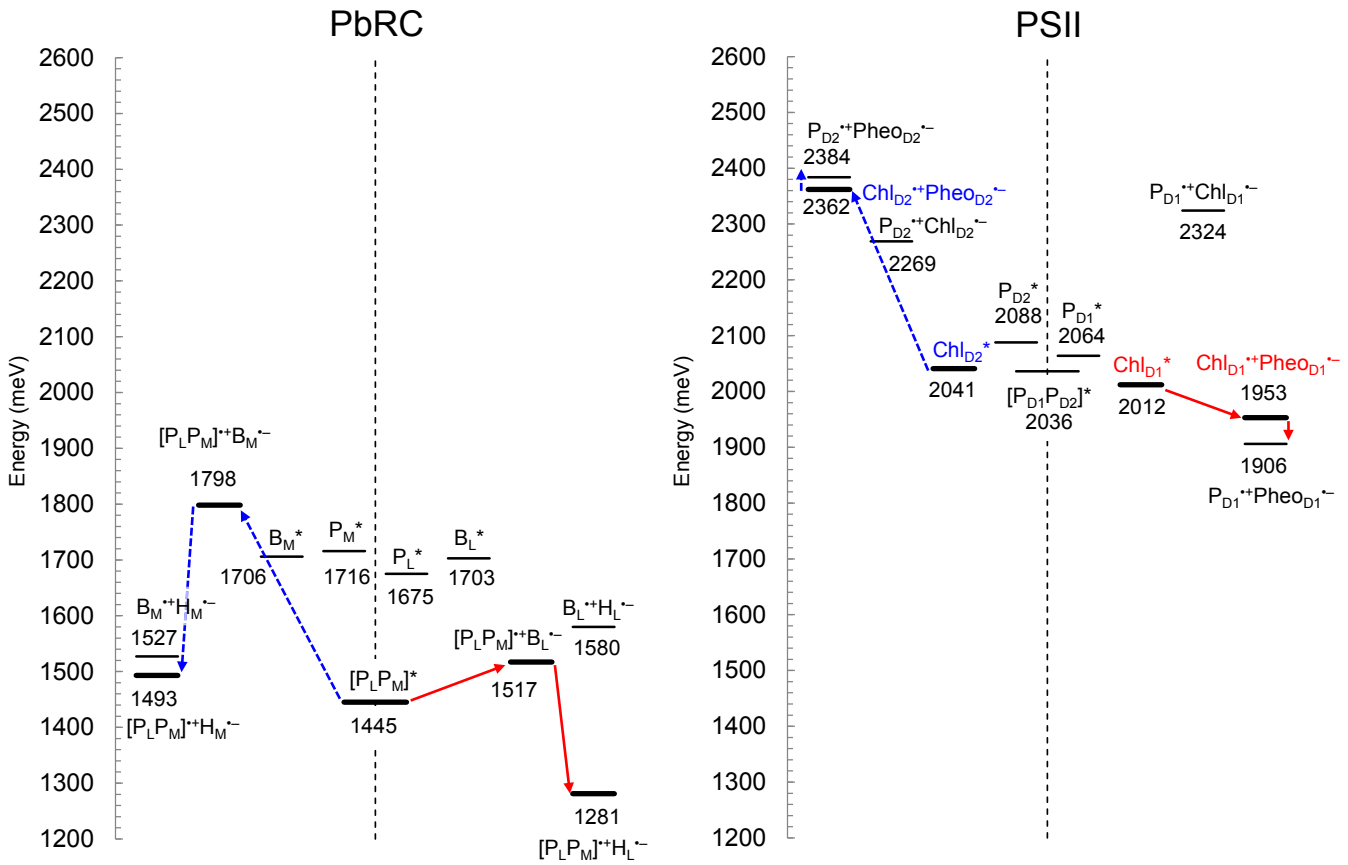

Fig. 2. Energy values for electronic excitation and charge-separated states of (bacterio)chlorophylls and (bacterio)pheophytins in PbRC (*Left*) and PSII (*Right*), calculated using a QM/MM approach, where the interaction between electron and hole was considered quantum-chemically. Thick solid bars indicate the major intermediate states. Red solid arrows indicate major electron transfer in the active branch, and blue dotted arrows indicate the corresponding electron transfer in the inactive branch.

crucial to the initial electron transfer (29): Mutations of Tyr-M210 to phenylalanine decreased the initial electron transfer with a time constant from 3.5 ps to 16 ps (20). The polar –OH group of Tyr-M210, which is oriented toward B_L, stabilizes the $B_L^{\bullet-}$ formation and increases $E_m(B_L)$ (19). The absence of the residue that corresponds to Tyr-M210 in PSII (i.e., D2-Leu205) (2) implies that there is a difference in the charge-separation mechanism between PbRC and PSII (discussed below). Thr-M186 is in van der Waals contact with the B_M chlorin ring. Because Thr-M186 forms an H-bond with the backbone carbonyl group of the ligand residue of B_M, His-M182, the hydroxyl O is oriented toward B_M, destabilizing $B_M^{\bullet-}$. Ser-L178 is located at a weak H-bond distance from the ester keto O of B_M (O…O = 3.5 Å). However, it forms an H-bond with the backbone carbonyl O of Met-L174 (O…O = 2.8 Å), which destabilizes $B_M^{\bullet-}$. Electrostatic interactions between these residues and B_M are pronounced in the hydrophobic protein environment near B_M, that is, ∼30 hydrophobic residues from subunit M that form the carotenoid binding site (19). All these residue pairs listed in Table 3 have already been suggested to stabilize $[P_LP_M]^{\bullet+}B_L^{\bullet-}$ with respect to $[P_LP_M]^{\bullet+}B_M^{\bullet-}$ in electrostatic calculations for PbRC (19).

The Absence of the Special Pair Chlorophylls in PSII. In contrast to $[P_LP_M]$ in PbRC, the calculated value of the excitonic coupling between P_{D1} and P_{D2} for the chlorophyll pair in PSII is small, 10 meV (Table 1). The electronic coupling between P_{D1} and P_{D2} is also very small, 13 meV, with respect to 114 meV between P_L and P_M in PbRC (Table 1). In addition, the highest occupied

Table 2. Factors that decrease the excitation energy of (bacterio)chlorophyll [(B)Chl] in the reaction center in millielectron volts

	B_M*	P_M*	P_L*	B_L*	Chl_{D2}*	P_{D2}*	P_{D1}*	Chl_{D1}*
(B)Chl* in vacuum	1,834	1,834	1,834	1,834	2,129	2,129	2,129	2,129
+Ring deformation[†]	−45	−48	−50	−67	−32	−3	−26	−37
+Protein electrostatics[‡]	−83	−70	−109	−64	−62	−38	−39	−85
(B)Chl* in protein without special pair formation	1,706	1,716	1,675	1,703	2,041	2,088	2,064	2,012
+Special pair formation[§]	0	−271	−230	0	0	0	0	0
(B)Chl* in protein	1,706	1,445	1,445	1,703	2,041	2,088	2,064	2,012

[†]Influence of deformation of the chlorin ring due to interactions with the protein environment (e.g., van der Waals contact and H-bond interactions).
[‡]Influence of electrostatic interactions with the protein environment.
[§]Influence of the formation of the special pair.

Table 3. L/M residue pairs that stabilize $B_L^{\bullet-}$ with respect to $B_M^{\bullet-}$ (>40 meV) in the LUMO energy level in millielectron volts, which corresponds to E_m for one-electron reduction

	$E_m(B_L)$	$E_m(B_M)$		$E_m(B_L)$	$E_m(B_M)$	Stabilizing $B_L^{\bullet-}$
Tyr-L67	5	0	Glu-M95*	−14	−141	132
Phe-L181	3	71	Tyr-M210	161	−5	98
Val-L157	30	0	Thr-M186	−3	−49	76
Ser-L178	5	−54	Ala-M207	−11	0	48
Asp-L155	−150	−35	Asp-M184*,†	−35	−193	43

*Cytochrome c_2 binding site (21).
†Corresponding to D1-Arg180 in PSII.

molecular orbital (HOMO) energy level of $[P_{D1}P_{D2}]$ is essentially the same as that of P_{D1}, whereas the LUMO energy level of $[P_{D1}P_{D2}]$ is the same as that of P_{D2} (Fig. 4*A*), suggesting that P_{D1} and P_{D2} do not form a special pair. Consistently, the HOMO–LUMO energy gap is correlated with the excitation energy in $[P_LP_M]$, but not in $[P_{D1}P_{D2}]$ (Fig. 4*B*). The absence of the $[P_{D1}P_{D2}]$ special pair is largely due to the low overlap of π-orbital between P_{D1} and P_{D2}. See *SI Appendix*, Table S2 for couplings of other excited states.

The Lowest Excitation-Energy Site, Chl_{D1}. Among P_{D1}, P_{D2}, $[P_{D1}P_{D2}]$, Chl_{D1}, and Chl_{D2}, the excitation energy of Chl_{D1} is the lowest (Fig. 2), as also indicated by the lowest HOMO–LUMO energy gap (Fig. 4*A*). The stretch in the chlorin ring along the Qy transition dipole moment may stretch in the π-conjugation system and decrease the excitation energy. The chlorin-ring deformation differs among P_{D1}, P_{D2}, Chl_{D1}, and Chl_{D2} (27). The N–N distance along the Qy transition dipole moment in the chlorin ring is longer in Chl_{D1} and Chl_{D2} than P_{D1} and P_{D2} (*SI Appendix*, Table S3 and Fig. S1). Accordingly, the N–N distance along the Qx transition dipole moment is shortest in Chl_{D1}. It seems likely that the N–N distance along the Qy transition dipole moment is partially associated with the excitation energy (*SI Appendix*, Fig. S1). However, it should also be noted that it does not explain the detailed difference, for example, between P_{D1} and P_{D2} (*SI Appendix, Supplementary Information Text*). The following factors contribute to the low excitation energy of Chl_{D1} with respect to other chlorophylls.

Low excitation energy at the accessory positions. P_{D1} and P_{D2} have histidine ligands (D1-His198 and D2-His197, respectively) and Chl_{D1} and Chl_{D2} have water ligands (W424D and W1009A, respectively). The difference in the ligand group, histidine or water, is not the primary reason for the lower excitation energy at the accessory chlorophyll sites than the pair chlorophyll sites, because two ligands decrease the chlorophyll excitation energy equally, by ∼10 meV (*SI Appendix*, Table S4).

Remarkably, the excitation energy of Chl_{D1} is decreased by the P_{D2} ligand, D2-His197, and a water molecule (W382D) that bridges between the Nδ site of D2-His197 and the keto O site of Chl_{D1} (*SI Appendix*, Table S4) because both -Nδ-H of D2-His197 and –OH of the bridging water molecule orient toward the keto O site of Chl_{D1} along the Qy transition dipole (Fig. 5*A*). On the Chl_{D2} site, the corresponding components, the P_{D1} ligand (D1-His198) and the bridging water molecule (W349A), also decrease the excitation energy (*SI Appendix*, Table S4). It seems that the H-bond network, $[P_{D2}...D2\text{-}His197...H_2O...Chl_{D1}]$ and $[P_{D1}...D1\text{-}His198...H_2O...Chl_{D2}]$, decrease the excitation energy on the accessory chlorophyll sites with respect to the pair chlorophyll sites.

The bridging water molecule is also conserved in PbRC. It may contribute to a decrease in the excitation energy at the accessory B_L and B_M sites. However, the influence can practically be ignored because the special pair $[P_LP_M]$ formation decreases the excitation energy at P_L and P_M more significantly in PbRC (>200 meV; Table 2).

Low excitation energy of Chl_{D1} with respect to Chl_{D2}. QM/MM calculations show that the difference in the protein electrostatic environment between D1 and D2 is the major factor that decreases the excitation energy of Chl_{D1} with respect to Chl_{D2} (by 23 meV; Table 2). Most of the D1/D2 residue pairs that stabilize Chl_{D1}* with respect to Chl_{D2}* are located at the van der Waals distance from Chl_{D1} and Chl_{D2}. D1-Met172, which is 3.7 Å away from Chl_{D1} in the loop region near helix ***cd*** (D1-176 to 190 and D2-176 to 188 in PSII, Fig. 3*B*), stabilizes Chl_{D1}* by 10 meV (Table 4) by hybridizing the sulfur lone-pair molecular orbital with the HOMO of Chl_{D1} (Fig. 5*B*) and interacting electrostatically. The corresponding stabilization is absent in Chl_{D2}* because D1-Met172 is replaced with D2-Pro171 near Chl_{D2}. As far as we are aware, the role of D1-Met172 in the PSII function is not reported, but the absence of the corresponding methionine near B_L in PbRC implies that D1-Met172 plays a role in stabilizing Chl_{D1}* in PSII, and that the charge separation mechanism differs between the two type-II reaction centers. D1-Met172 is replaced with leucine in the PsbA2 protein, which can be expressed under microaerobic conditions in cyanobacterial PSII. In PsbA2, in turn, the next residue D1-Pro173 is replaced with methionine (30), which might partially substitute a role of D1-Met172 of the PsbA protein. The difference in the H-bond network of the ligand water molecule between Chl_{D1} and Chl_{D2}, i.e., the presence of an H-bond donor (D1-Thr179) on the Chl_{D1} side and the

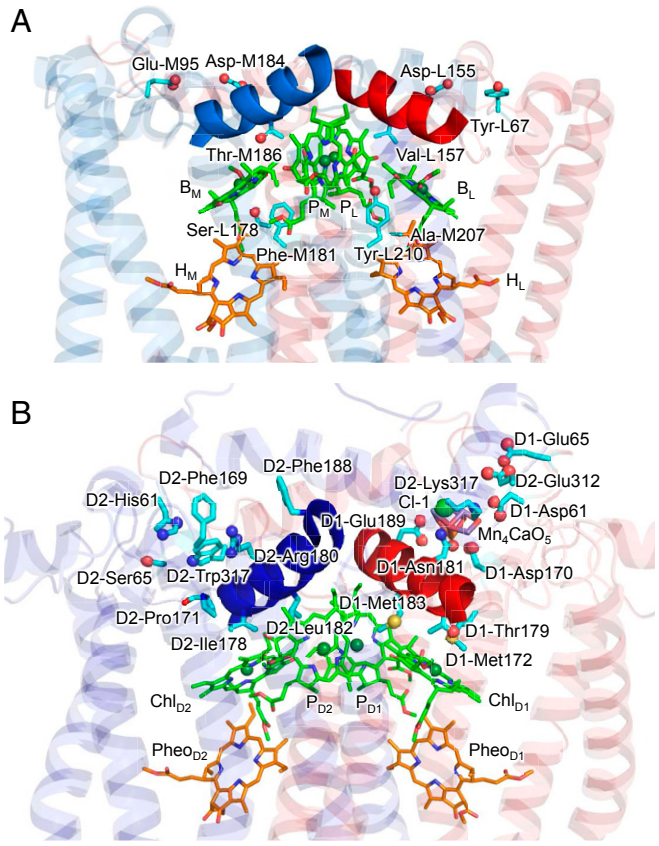

Fig. 3. (*A*) L/M residue pairs that stabilize $B_L^{\bullet-}$ with respect to $B_M^{\bullet-}$ in PbRC. Most of the residue pairs are located in the hydrophobic transmembrane region. Helix ***cd*** in L and M are colored red and blue, respectively. (*B*) D1/D2 residue pairs that stabilize $Chl_{D1}^{\bullet+}Pheo_{D1}^{\bullet-}$ with respect to $Chl_{D2}^{\bullet+}Pheo_{D2}^{\bullet-}$ or that stabilize Chl_{D1}* with respect to Ch_{lD2}* in PSII. In contrast to PbRC, most of the residue pairs are located in the membrane-extrinsic region. Helix ***cd*** in D1 and D2 are colored red and blue, respectively.

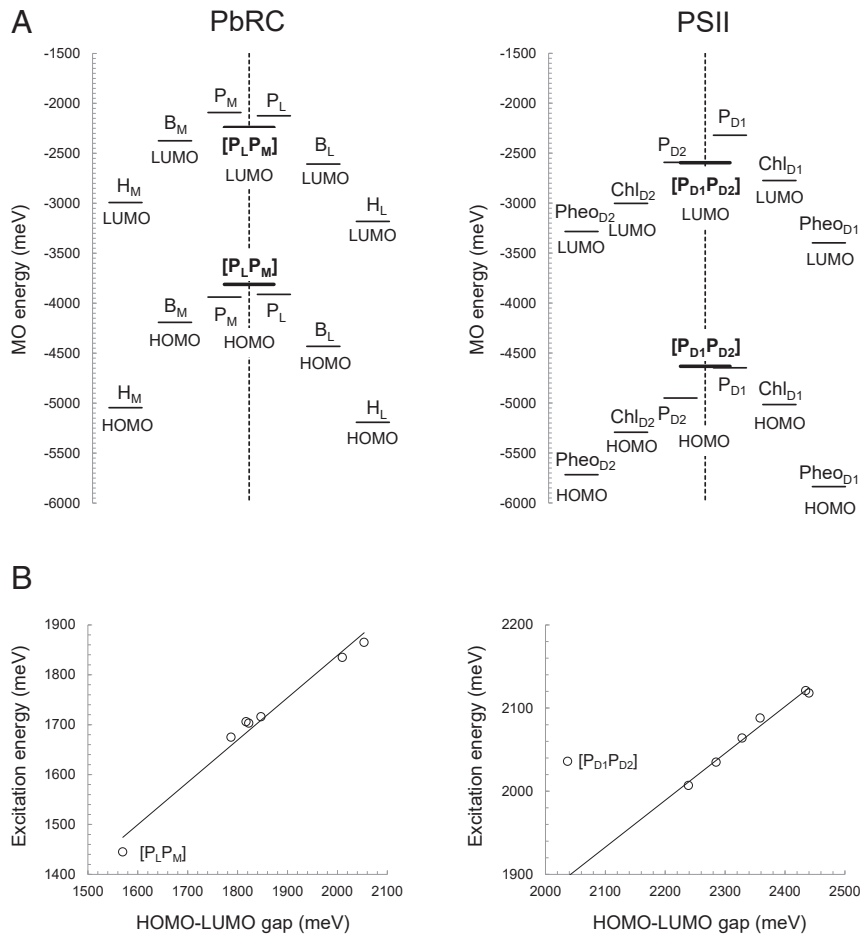

Fig. 4. (*A*) LUMO and HOMO energy levels in PbRC (*Left*) and PSII (*Right*) in millielectron volts, calculated including the four (bacterio)chlorophylls and two (bacterio)pheophytins in the QM regions. Thick bars indicate $[P_LP_M]$ and $[P_{D1}P_{D2}]$. (*B*) Correlation between calculated HOMO–LUMO gap and excitation energy in PbRC (*Left*) (coefficient of determination $R^2 = 0.98$) and PSII (*Right*) ($R^2 = 0.98$, excluding $[P_{D1}P_{D2}]$). $[P_{D1}P_{D2}]$ does not fit to the correlation, because excitation of $[P_{D1}P_{D2}]$ is excitation from HOMO of P_{D1} to LUMO of P_{D2} (A), which corresponds to charge transfer process, that is, the $P_{D1}^{\bullet+}P_{D2}^{\bullet-}$ formation.

absence of the H-bond donor (D2-Ile178) on the Chl_{D2} side also decreases the excitation energy of specifically Chl_{D1} (4 meV; Table 4).

The only electrostatic component that decreases the excitation energy of Chl_{D1} with respect to Chl_{D2} is Cl-1 and the binding sites D1-Asn181 and D2-Lys317 (2 meV; Table 4 and Fig. 3*B*). Molecular dynamics simulations by Rivalta et al. (31) suggested that the removal of Cl-1 from the binding site lead to the formation of a salt-bridge between D1-Asp61 and D2-Lys317; this would inhibit the release of a proton from W1. The counterpart of polar D1-Asn181 is basic D2-Arg180, which provides a driving force for proton transfer from TyrD toward the bulk surface (32, 33). Mutations of D2-Arg180 resulted in a loss and/or serious modifications of the electron paramagnetic resonance signal from TyrD and perturbations in the PSII photochemistry (34). The D1-Asn181/D2-Arg180 pair also contributes to $P_{D1}^{\bullet+} > P_{D2}^{\bullet+}$ (8) and $E_m(Chl_{D1}) < E_m(Chl_{D2})$ (i.e., $Chl_{D1}^{\bullet+} > Chl_{D2}^{\bullet+}$) (19). See below for further details of the D1-Asn181/D2-Arg180 pair.

Charge-Separated State $Chl_{D1}^{\bullet+}Pheo_{D1}^{\bullet-}$ in PSII. As described, Chl_{D1} has the lowest excitation energy among the four chlorophylls and can serve as the initial electron donor. In this case, $Chl_{D1}^{\bullet+}Pheo_{D1}^{\bullet-}$ is the initial charge-separated state. In the TDDFT-QM/MM/PCM calculations, where the interaction between electron and hole is considered quantum-chemically, $Chl_{D1}^{\bullet+}Pheo_{D1}^{\bullet-}$ in the D1-branch is 409 meV is more stable than the corresponding $Chl_{D2}^{\bullet+}Pheo_{D2}^{\bullet-}$ in the D2-branch, which suggests that the charge separation occurs predominantly along the D1-branch via $Chl_{D1}^{\bullet+}Pheo_{D1}^{\bullet-}$ (Fig. 2). The HOMO energy level is highest at P_{D1} among the four chlorophylls (Fig. 4*A*). This indicates that the hole on $Chl_{D1}^{\bullet+}Pheo_{D1}^{\bullet-}$ is transferred to and stabilized predominantly at P_{D1}, which is consistent with the larger population of $P_{D1}^{\bullet+}$ than $P_{D2}^{\bullet+}$ in the $[P_{D1}P_{D2}]^{\bullet+}$ pair (8, 35–37). The significant energy difference between $Chl_{D1}^{\bullet+}Pheo_{D1}^{\bullet-}$ and $Chl_{D2}^{\bullet+}Pheo_{D2}^{\bullet-}$ is mainly due to the energy difference in the oxidized accessory chlorophylls, $Chl_{D1}^{\bullet+}$ and $Chl_{D2}^{\bullet+}$ (272 meV), rather than in the reduced pheophytins, $Pheo_{D1}^{\bullet-}$ a and $Pheo_{D2}^{\bullet-}$ (114 meV, *SI Appendix*, Fig. S3).

Larger stability of $Pheo_{D1}^{\bullet-}$ than $Pheo_{D2}^{\bullet-}$. The D1/D2 residue pairs that stabilize $Pheo_{D1}^{\bullet-}$ with respect to $Pheo_{D2}^{\bullet-}$ were D1-Met214/D2-Ile213 (106 meV), D1-Arg27/D2-Phe27 (73 meV), D1-Tyr126/D2-Phe125 (67 meV), and D1-Arg136/D2-Leu135 (52 meV) (Table 5). D1-Met214 provides the hydrophobic binding pocket to the isoprenoid side-chain of Q_B. D1-Met214 destabilizes $Pheo_{D2}^{\bullet-}$ ($S_{D1\text{-}Met214}\cdots O_{PheoD2} = 3.1$ Å) in the hydrophobic environment, whereas the Cγ of D2-Ile213 stabilizes $Pheo_{D1}^{\bullet-}$ ($C\gamma_{D2\text{-}Ile213}\cdots O_{PheoD1} = 3.1$ Å; Table 5). D1-Arg27 stabilizes the binding of the anionic head group of sulfoquinovosyl diacylglycerol. Although D1-Arg27 and D1-Arg136 are located near the stromal surface, their electrostatic influence is not

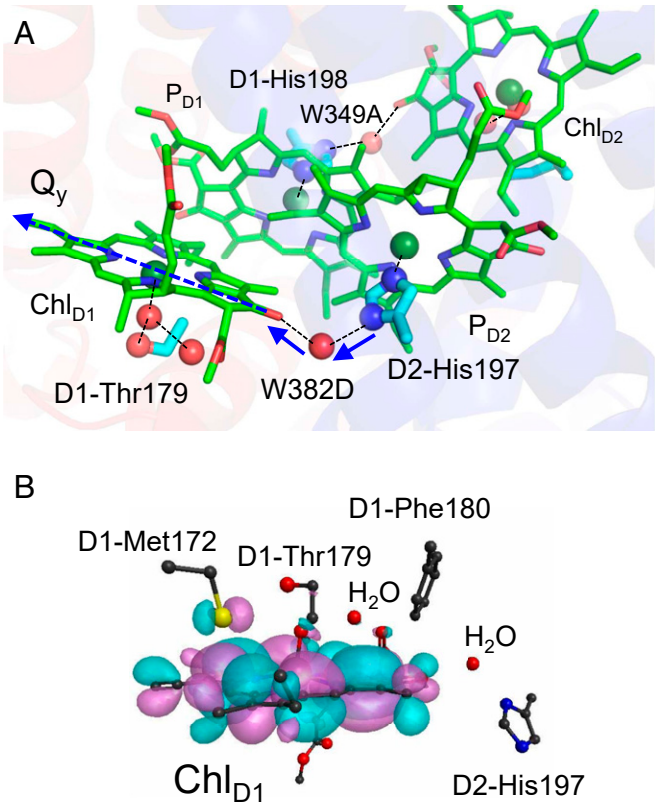

Fig. 5. (*A*) The bridging water molecule (W382D) that connects between the ligand Nδ site of P_{D2} and the keto O site of Chl_{D1}. H-bonds and ligand interactions are indicated by dotted lines. The donor to acceptor orientations of the H-bonds are indicated by blue solid arrows. The Qy transition dipole is indicated by the dotted blue arrow (see *SI Appendix*, Fig. S1 for the orientations of the Qx and Qy transition dipoles). (*B*) Distribution of HOMO (pink and cyan spaces) at the Chl_{D1} moiety, which were obtained based on QM/MM/PCM (r = 3.0) with the CAM-B3LYP functional (μ = 0.14). The QM region was defined as Chl_{D1}, the ligand (W424D), second sphere ligand (W1003A), and bridging (W382D) water molecules, and the side chains of D1-Met172 and D1-Phe180 in van der Waals contact with Chl_{D1}, and the ligand (or ligand-associated) side chains of D1-Thr179 and D2-His197.

completely shielded at $Pheo_{D1}$ due to the presence of the hydrophobic environment around Q_A. D1-Tyr126 donates an H-bond to the ester carbonyl O of $Pheo_{D1}$ and stabilizes $Pheo_{D1}^{\bullet-}$ (38).

In PbRC, $H_L^{\bullet-}$ is also more stable than $H_M^{\bullet-}$ (Figs. 2 and 4). However, the L/M residues that stabilize $H_L^{\bullet-}$ with respect to $H_M^{\bullet-}$ (e.g., Glu-L104 (39), *SI Appendix*, Table S5) do not correspond to those that stabilize $Pheo_{D1}^{\bullet-}$ with respect to $Pheo_{D2}^{\bullet-}$ (Table 5), which implies the difference in the protein electrostatic environment and the charge-separation mechanism between the two reaction centers.

Larger stability of $Chl_{D1}^{\bullet+}$ than $Chl_{D2}^{\bullet+}$. The D1-Asp61/D2-His61 and D1-Asp170/D2-Phe169 pairs stabilize $Chl_{D1}^{\bullet+}$ with respect to $Chl_{D2}^{\bullet+}$ (Table 6 and Fig. 3*B*); the two residue pairs are reported to be responsible for the lower $E_m(Chl_{D1})$ than $E_m(Chl_{D2})$ (19). The D1-Met172/D2-Pro171 and D1-Thr179/D2-Ile178 pairs stabilize not only $Chl_{D1}^{\bullet+}$ with respect to $Chl_{D2}^{\bullet+}$ (Table 6 and Fig. 3*B*) but also Chl_{D1}^{*} with respect to Chl_{D2}^{*} (Table 4), facilitating the Chl_{D1}^{*} formation and the subsequent $Chl_{D1}^{\bullet+}$ formation. Remarkably, many of the residues listed in Table 6 play a key role in the release of electrons or protons from the substrate water molecules. D1-Asp61/D2-His61, D1-Asn181/D2-Arg180, and D1-Asp170/D2-Phe169 contribute to $P_{D1}^{\bullet+} > P_{D2}^{\bullet+}$ (8), which is advantageous for electron transfer from the substrate water molecules to $P_{D1}^{\bullet+}$. D1-Asp61 (32, 40–43), D2-Lys317 (31, 44), and Cl^- (32, 45, 46) are involved in the proton transfer pathway that proceeds from the oxygen-evolving complex toward the protein bulk surface. D1-Asp170 and D1-Glu189 listed in Table 6 are the ligand residues of the Mn_4CaO_5 cluster.

$P_{D1}^{\bullet+}Pheo_{D1}^{\bullet-}$ in PSII. Fig. 2 shows that $P_{D1}^{\bullet+}Pheo_{D1}^{\bullet-}$ is more stable than $Chl_{D1}^{\bullet+}Pheo_{D1}^{\bullet-}$, which suggests that the hole on $Chl_{D1}^{\bullet+}$ is transferred to $P_{D1}^{\bullet+}$ during the charge-separation process. Because P_{D1} is closer to TyrZ than Chl_{D1}, the $P_{D1}^{\bullet+}$ formation is more advantageous to accept an electron from the substrate water molecules via TyrZ in water oxidation. The corresponding state on the D2 side, $P_{D2}^{\bullet+}Pheo_{D2}^{\bullet-}$, is 478 meV less stable than $P_{D1}^{\bullet+}Pheo_{D1}^{\bullet-}$, which suggests that the charge separation predominantly occurs along the D1-branch and the charge separation via $Chl_{D1}^{\bullet+}Pheo_{D1}^{\bullet-}$ is further stabilized by the $P_{D1}^{\bullet+}Pheo_{D1}^{\bullet-}$ formation (Fig. 2).

Discussion

The present result indicates that the absence of the special pair formation between P_{D1} and P_{D2} prevents $[P_{D1}P_{D2}]$ from serving the initial electron donor, but it increases E_m for one-electron oxidation and makes PSII capable of oxidizing the substrate water molecules (11, 47). The absence of the special pair formation along the pseudo-C_2 axis also requires PSII to localize the initial charge separation site either on the D1 or D2 side. The excitation energy is lowest at Chl_{D1}, although the difference in the energy between Chl_{D1}^{*} and Chl_{D2}^{*} is not particularly large, 29 meV (Fig. 2). The initial charge-separated state, $Chl_{D1}^{\bullet+}Pheo_{D1}^{\bullet-}$, is 409 meV more stable than $Chl_{D2}^{\bullet+}Pheo_{D2}^{\bullet-}$ (Fig. 2) due to the more positively charged protein environment on the D2 side than on the D1 side (e.g., D1-Asp61/D2-His61, D1-Asn181/D2-Arg180, and D1-Trp317/D2-Lys317 in Table 6 (19)). In the presence of the intramolecular reorganization energy, the corresponding energy difference is 386 meV; charge separation from $[Chl_{D1}]^{*}$ to $Ch_{D1}^{\bullet+}Pheo_{D1}^{\bullet-}$ is 264 meV energetically downhill, whereas charge separation from $[Chl_{D2}]^{*}$ to $Ch_{D2}^{\bullet+}Pheo_{D2}^{\bullet-}$ is 95 meV uphill (*SI Appendix*, Fig. S2), in agreement with electron transfer predominantly occurring along the D1 branch.

Remarkably, many of these residues that play a key role in stabilizing Chl_{D1}^{*} (Table 4) and $Chl_{D1}^{\bullet+}$ (Table 6) are located in the lumenal helix ***cd*** (D1-176 to 190 and D2-176 to 189) and adjacent loop (D1-166 to 175 and D2-164 to 175) region (Fig. 3*B*). It has been reported that the lumenal helix ***cd*** and adjacent loop region characterizes PSII with respect to PbRC most significantly, making $E_m(Chl_{D1}) < E_m(Chl_{D2})$ in PSII, whereas $E_m(B_L) > E_m(B_M)$ in PbRC (19). Two Mn_4CaO_5 ligand residues, D1-Asp170 and D1-Glu189, are also located in this region and stabilize $Chl_{D1}^{\bullet+}$ (Table 6). Intriguingly, in the earliest-evolving D1 proteins (e.g., *Gloeobacter kilaueensis*, *Chroococcidiopsis thermalis* PCC7203, and *Fischerella* sp. JSC-11), the two ligand residues are not conserved (48). D1-Asp170 is replaced with alanine or serine, which would fail to bind Ca^{2+} and the dangling Mn (Mn4). D1-Glu189 is often replaced with aspartate (asparagine,

Table 4. D1/D2 residue pairs that decreases the excitation energy of Chl_{D1} with respect to Chl_{D2} in millielectron volts

	Chl_{D1}*	Chl_{D2}*		Chl_{D1}*	Chl_{D2}*	Stabilizing Chl_{D1}*
D1-Met172	−10	0	D2-Pro171	0	1	−11
D1-Thr179	−4	0	D2-Ile178	0	0	−4
Cl-1	−2	0				−2[†]
+D1-Asn181	0	0	+D2-Arg180	0	2	
+D1-Trp317	0	0	+D2-Lys317	2	0	

[†]As a Cl-1 binding site with Cl-1, D1-Asn181, and D2-Lys317.

Table 5. D1/D2 residue pairs that stabilize $Pheo_{D1}^{\bullet-}$ with respect to $Pheo_{D2}^{\bullet-}$ (>40 meV) in the LUMO energy level in millielectron volts (corresponding to E_m for one-electron reduction)

	$E_m(Pheo_{D1})$	$E_m(Pheo_{D2})$		$E_m(Pheo_{D1})$	$E_m(Pheo_{D2})$	Stabilizing $Pheo_{D1}^{\bullet-}$
D1-Met214	8	−41	D2-Ile213	65	8	106
D1-Arg27	84	19	D2-Phe27	0	−8	73
D1-Tyr126	84	3	D2-Phe125	0	14	67
D1-Arg136	71	14	D2-Leu135	0	5	52

arginine, glutamine, or alanine in some D1 proteins) in the earliest-evolving D1 proteins. The side chain of D1-Glu189 accepts an H-bond from a water molecule (W7), which is the H-bond donor to TyrZ and is required for TyrZ and D1-His190 to form a remarkably short, low-barrier H-bond ($O_{TyrZ}\cdots N_{D1\text{-}His190}$ = 2.5 Å) (49). Shortening the side-chain length from glutamate to aspartate would alter the W7 position and fail to form the low-barrier H-bond. Based on these, the earliest evolving D1 proteins are unlikely to proceed water oxidation (48). Indeed, the earliest evolving D1 proteins also lack D1-Glu65 in the proton transfer pathway (40, 41, 50), which suggests that not only the Mn_4CaO_5 cluster but also the proton transfer pathway is incomplete.

In contrast, the protein environment near $Pheo_{D1}$ is highly conserved even in the earliest evolving D1 proteins, as D1-residues listed in Table 5 are mostly conserved (note that D1-Met214 is replaced with alanine in *G. kilaueensis*) (48). In addition, the D1/D2 residue pairs that facilitate the $Pheo_{D1}^{\bullet-}$ formation (Table 5) are neither in common with the residue pairs that facilitate the Chl_{D1}* formation (Table 4) nor the $Chl_{D1}^{\bullet+}$ formation (Table 6). It seems thus far likely that the acquirement of the oxygen-evolving ability predominantly alters the protein environment that is crucial specifically for the Chl_{D1}, without affecting the $Pheo_{D1}$ energetics.

The difference in the electrostatic properties of the residues that stabilize the charge-separated intermediate states between PbRC and PSII is also remarkable. In PSII, charged residues are predominantly involved in the stabilization of $Chl_{D1}^{\bullet+}Pheo_{D1}^{\bullet-}$ (Table 6), whereas in PbRC, polar, uncharged residues are involved in the stabilization of $[P_LP_M]^{\bullet+}B_L^{\bullet-}$ (Table 3). Because the binding sites of Chl_{D1} and B_L are located in the uncharged transmembrane regions, the stabilization of $[P_LP_M]^{\bullet+}B_L^{\bullet-}$ by polar, uncharged residues is energetically favored. The less-charged protein environment of PbRC is also indicated as Glu-M95 on the protein surface of subunit M destabilizes not only $B_M^{\bullet-}$ (Table 3) but also $H_M^{\bullet-}$ (*SI Appendix*, Table S5). These polar, uncharged residues are not conserved in PSII. It is highly likely that the membrane-extrinsic charged region that provides the cationic Mn_4CaO_5 binding site and the proceeding proton transfer pathway can stabilize the charge-separated state more effectively (e.g., PSII) than the polar protein environment in the uncharged transmembrane region (e.g., PbRC). This could also explain why PSII does not require Tyr-M210, the residue that is most crucial to the stabilization of $[P_LP_M]^{\bullet+}B_L^{\bullet-}$ (19, 20, 29).

Conclusions

Based on the energetics of the electronically excited states and charge-separated states presented here, we are able to explain why electron transfer predominantly occurs along the L-branch in PbRC and the D1-branch in PSII, irrespective of the pseudo-C_2 symmetry of the two electron transfer branches (Fig. 2). Notably, these findings cannot be obtained solely from the E_m profiles, as the LUMO energy levels (i.e., E_m for one-electron reduction) are downhill along the two branches in both PbRC and PSII (Fig. 4*A*).

In PbRC, P_L and P_M form the special pair $[P_LP_M]$, as indicated by a decrease of 230 to 270 meV in the excitation energy (Table 2 and Fig. 2). $[P_LP_M]^{\bullet+}B_L^{\bullet-}$ is 281 meV more stable than $[P_LP_M]^{\bullet+}B_M^{\bullet-}$ (Fig. 2). Glu-M95 and Asp-M184, which provide the cytochrome c_2 binding interface (21), are the charged components that destabilize $B_M^{\bullet-}$. In contrast to PSII, it is characteristic to PbRC

Table 6. D1/D2 residue pairs that stabilize $Chl_{D1}^{\bullet+}$ with respect to $Chl_{D2}^{\bullet+}$ (>40 meV) in the HOMO energy level in millielectron volts (corresponding to E_m for one-electron oxidation)

	$E_m(Chl_{D1})$	$E_m(Chl_{D2})$		$E_m(Chl_{D1})$	$E_m(Chl_{D2})$	Stabilizing $Chl_{D1}^{\bullet+}$
D1-Asp61*	−117	−35	D2-His61[†]	35	141	−188
Cl-1	−152	−57				−141[‡]
+D1-Asn181[†]	14	0	+D2-Arg180[†]	68	234	
+D1-Trp317	−5	−5	+D2-Lys317[§]	152	46	
D1-Thr179[¶]	−35	−5	D2-Ile178	−8	52	−90
D1-Asp170[#]	−122	−44	D2-Phe169	−5	−11	−72
D1-Met183	−19	3	D2-Leu182	−5	35	−62
D1-Arg323	38	65	D2-Glu323	−82	−52	−57
D1-Asp59	−73	−22	D2-Tyr59	0	3	−54
D1-Met172	−22	0	D2-Pro171	5	35	−52
D1-Glu65[‖]	−79	−19	D2-Ser65	−3	−8	−55
+D1-Asn315			+D2-Glu312[‖]			
D1-Glu189[#]	−79	−41	D2-Phe188	3	14	−49
D1-Val306	0	0	D2-Glu302	−87	−38	−49

*Proton transfer pathway proceeding from the Mn_4CaO_5 cluster.
[†]Proton transfer pathway proceeding from TyrD (32, 33, 61), corresponding to Asp-M184 in PbRC.
[‡]As a Cl-1 binding site with Cl-1, D1-Asn181, and D2-Lys317.
[§]Cl-1 binding site.
[¶]H-bond partner of the second sphere water ligand of Chl_{D1}.
[#]Ligand of the Mn_4CaO_5 cluster.
[‖]Water channel (50, 62) and proton transfer pathway proceeding from the Mn_4CaO_5 cluster (41, 63).

that polar residues in der van der Waals contact with B_L and B_M also contribute to the significant energy difference between $[P_LP_M]^{\bullet+}B_L^{\bullet-}$ and $[P_LP_M]^{\bullet+}B_M^{\bullet-}$. Tyr-M210 stabilizes $B_L^{\bullet-}$, and Thr-M186 and Ser-L178 destabilize $B_M^{\bullet-}$ (Table 3). The values of electronic coupling and excitonic coupling between P_{D1} and P_{D2} in PSII are significantly smaller than those between P_L and P_M in PbRC (Table 1), which indicates that P_{D1} and P_{D2} do not form the special pair. The absence of the special pair in PSII displaces the excitation site from the pseudo-C_2 axis to the D1 site. The H-bond network [P_{D2}...D2-His197...H_2O...Chl_{D1}] and [P_{D1}...D1-His198...H_2O...Chl_{D2}], which orients toward the Qy transition dipole of Chl_{D1} and Chl_{D2}, decrease the excitation energy of Chl_{D1} and Chl_{D2}, respectively (*SI Appendix*, Table S4 and Fig. 5*A*). The presence of D1-Met172 that hybridizes the sulfur lone-pair molecular orbital with the HOMO of Chl_{D1} (Fig. 5*B*) and D1-Thr179 that forms the H-bond network with the Chl_{D1} ligand water molecule contribute to a decrease in the excitation energy of Chl_{D1} (Table 4). The excitation energy of Chl_{D1} is thus far slightly (29 meV) lower than that of Chl_{D2} (Fig. 2), whereas $Chl_{D1}^{\bullet+}Pheo_{D1}^{\bullet-}$ is 409 meV more stable than $Chl_{D2}^{\bullet+}Pheo_{D2}^{\bullet-}$ (*SI Appendix*, Fig. S3). This suggests that the large stability of $Chl_{D1}^{\bullet+}Pheo_{D1}^{\bullet-}$ is the main factor that facilitates the D1-branch electron transfer. The large stability of $P_{D1}^{\bullet+}Pheo_{D1}^{\bullet-}$ with respect to $Chl_{D1}^{\bullet+}Pheo_{D1}^{\bullet-}$ (Fig. 2) makes $P_{D1}^{\bullet+}$ serve as an electron acceptor for the substrate water molecules via TyrZ.

In PSII, the key components that play a role in stabilizing the intermediate $Chl_{D1}^{\bullet+}$ state and facilitating the D1-branch electron transfer (Table 6) also play a role in 1) decreasing the excitation energy of Chl_{D1} (D1-Met172, D1-Thr179, and Cl-1; Table 4), 2) constructing the Mn_4CaO_5 cluster (D1-Asp170, D1-Glu189, and the second sphere ligand D1-Asp61; Table 6), 3) mediating proton transfer from the substrate water molecules [D1-Asp61, D1-Glu65, D2-Glu312, and Cl-1 (41, 51)], and 4) facilitating electron transfer from the substrate water molecule by pushing the cationic state toward $P_{D1}^{\bullet+}$ [D1-Asp61/D2-His61, D1-Asp170/D2-Phe169, D1-Asn181/D1-Arg180, and D1-Glu189/D2-Phe188 (8)]. Thus, the charge-separation mechanism, the Chl_{D1}^* formation and the subsequent electron transfer via the $Chl_{D1}^{\bullet+}$ intermediate, is largely associated with the water-splitting ability.

As viewed, the localization of the acidic environment for hosting the Mn_4CaO_5 cluster (e.g., the Mn_4CaO_5 ligands and the proceeding proton transfer pathway) contributes to the $Chl_{D1}^{\bullet+}Pheo_{D1}^{\bullet-}$ stabilization in the charge separation process (Table 6). This can explain why both the water-splitting site and the charge-separation site are located on the same D1 protein. The localization of the acidic environment for hosting the Mn_4CaO_5 cluster also contributes to the $P_{D1}^{\bullet+}$ stabilization in the $[P_{D1}P_{D2}]^{\bullet+}$ pair (8). This also indicates that the localization of the Mn_4CaO_5 cluster on the D1 protein is ultimately the basis of restricting photodamage to the D1 protein (47). It should be noted that the absence of large π-coupling between P_{D1} and P_{D2} can also contribute to confining the subsequent cationic state to the D1 side (as $P_{D1}^{\bullet+}$).

Most of the D1/D2 residue pairs that facilitate the D1-branch electron transfer (Tables 4 and 6) are not conserved in PbRC (2) and some of these residues are even not conserved in the earliest evolving D1 proteins (48). Most of the L/M residue pairs that facilitate the L-branch electron transfer in PbRC (Table 3) are also not conserved in PSII (2). The independent components (i.e., uncharged polar groups near B_L and B_M in the transmembrane region in PbRC and charged groups near the water-splitting/proton-conducting site in the membrane-extrinsic region in PSII) facilitate the similar, unidirectional electron transfer in completely different mechanisms. It seems likely that the unique charge separation via $Chl_{D1}^{\bullet+}Pheo_{D1}^{\bullet-}$ is pronounced after PSII obtains the complete, functional Mn_4CaO_5 cluster and the proceeding electron and proton transfer pathways.

Methods

Coordinates and Atomic Partial Charges. The atomic coordinates were taken from the X-ray structures, PbRC from *R. sphaeroides* at 2.01-Å resolution (Protein Data Bank [PDB] ID code 3I4D), and PSII monomer unit (designated monomer A) of the PSII complexes from *Thermosynechococcus vulcanus* at 1.9-Å resolution (PDB ID code 3ARC) (52). The polarizable AMBER-02 force field (53) was used to consider the induced dipoles of the MM atoms. The positions of all heavy atoms were fixed and all titratable groups (e.g., acidic and basic groups) were ionized in the MM region. The residue protonation states were consistent with those used for E_m calculations in PbRC and PSII (19). The protonation states of the titratable residues were considered to be ionized for acidic and basic residues and charge-neutral for histidine residues unless otherwise specified (listed in ref. 50). Because D1/D2 residue pairs that affect the excitation energy (Table 4) or the charge-separated state (Table 6) do not contain the doubly protonated histidine residues [e.g., D1-His92 (50)] except for D2-His61, the present results are unlikely to depend on the protonation states. The large stability of $Chl_{D1}^{\bullet+}$ with respect to $Chl_{D2}^{\bullet+}$ will be less pronounced if D2-His61 is not doubly protonated. However, this does not affect the conclusions, because D1-Asp61 is ionized (41). D1-His337, which forms an H-bond with the Mn_4CaO_5 cluster, was considered to be protonated (54). Water molecules in the crystal structures were represented explicitly. The atomic charges of the other cofactors [(bacterio)chlorophyll, (bacterio)pheophytin, ubiquinone, plastoquinone, spheroidene, sulfoquinovosyl diacylglycerol, heptyl 1-thiohexopyranoside, and the Fe complex] were taken from previous studies (19), which were determined by fitting the electrostatic potential in the neighborhood of these molecules using the RESP (Restrained Electrostatic Potential) procedure (55). To obtain the atomic charges of the Mn_4CaO_5 cluster or the Fe complex, backbone atoms are not included in the RESP procedure (except for D1-Ala344). The resulting atomic partial charges of the cofactors, including the nonheme Fe complex in PbRC and PSII and the Mn_4CaO_5 cluster (S_1), where (Mn1, Mn2, Mn3, Mn4) = (III, IV, IV, III), are listed in ref (19). For the atomic charges of the nonpolar CH_n groups in cofactors (e.g., the phytol chains of (bacterio)chlorophyll and (bacterio)pheophytin and the isoprene side chains of quinones), the value of +0.09 was assigned for nonpolar H atoms.

QM/MM Calculations. We employed the electrostatic embedding QM/MM/PCM scheme for all of the electronic structure calculations. We used the QuanPol method (56) implemented in the GAMESS code (57), in which Lennard-Jones parameters describe interactions between QM and MM atoms.

Geometry Optimization. For geometry optimization, the DFT method was employed with the B3LYP functional plus the Grimme's dispersion correction (58) and 6-31G(d) basis sets. The PCM method was not used for geometry optimization (i.e., QM/MM). All of the atomic coordinates in the QM region were fully relaxed (i.e., not fixed) during the QM/MM-geometry optimization. The coordinates of the heavy atoms in the surrounding MM region were fixed at their original X-ray coordinates. The polarizable AMBER-02 force field (53) was used to consider the induced dipoles of the MM atoms and to reproduce the dielectric screening. For geometry optimization of (bacterio)chlorophyll, the QM region was defined as the $P_L/P_M/B_L/B_M$ bacteriochlorophyll tetramer for PbRC and the $P_{D1}/P_{D2}/Chl_{D1}/Chl_{D2}$ chlorophyll tetramer for PSII, with the ligand groups and the water molecules as an H-bond partner of (bacterio)chlorophyll. The H-bond partners of (bacterio)chlorophylls and (bacterio)pheophytins (i.e., His-L168 for P_L, protonated Glu-L104 for H_L, D1-Tyr126 and D1-Gln130 for $Pheo_{D1}$, and D2-Gln129 and D2-Asn142 for $Pheo_{D2}$) were also included in the QM region. See Datasets S1 and S2 for the QM/MM-optimized atomic coordinates.

Contribution of Residues to the HOMO and LUMO Energy Levels. To analyze contributions of residues to the HOMO and LUMO levels (which correspond to E_m for one-electron oxidation and reduction, respectively), we used the QM/MM/PCM scheme with the B3LYP functional (i.e., polarizable QM/MM/PCM).

Electronic Coupling, Excitonic Coupling, Excited States, and Charge-Separated States. To calculate electronic coupling of the (bacterio)chlorophyll pair, we employed a QM/MM approach with PCM method with the dielectric constant of 80, in which electrostatic and steric effects created by a protein

environment were explicitly considered in the presence of bulk water. Here, the polarizable amber-02 force field (53) was applied for the MM region, where induced dipoles of the MM atoms were considered to reproduce the dielectric screening (i.e., polarizable QM/MM/PCM). In the PCM method, the polarization points were put on the spheres with the radius of 3.0 Å from each atom center. The intramolecular reorganization energies of (bacterio) chlorophylls were calculated through QM/MM-geometry optimization.

To analyze excitonic coupling of the (bacterio)chlorophyll pair and the energetics of electronically excited states and charge separated states, the TDDFT was employed with the CAMB3LYP functional (59), where the range-separation parameters μ of 0.14 (25), α of 0.19, and β of 0.46 were used (i.e., polarizable TDDFT-QM/MM/PCM). The electronic couplings between excited states are calculated with the diabatization scheme of adiabatic electronic states (28). Here, the exciton coupling includes contributions from both long-range Coulomb (Förster) and electron exchange (Dexter) mechanisms. When excited states were not involved in the electronic coupling between the pair (bacterio)chlorophylls, charge transfer integrals were calculated based on (bacterio)chlorophyll monomer orbitals and the Fock matrix of (bacterio)chlorophyll dimer (60). The calculation scheme for the electronic coupling (28) is implemented in the modified version of the GAMESS program.

Data Availability. All of the data supporting the findings of this study are available within the paper, *SI Appendix*, and Datasets S1 and S2.

ACKNOWLEDGMENTS. This research was supported by Japan Science and Technology Agency Core Research for Evolutional Science and Technology (JPMJCR1656 to H.I.), Japan Society for the Promotion of Science Grants-in-Aid for Scientific Research (JP18H01937 to H.T. and H.I., JP18H05155, JP20H03217, and JP20H05090 to H.I., JP18H01186 to K.S., and JP16H06560 to K.S.), and the Interdisciplinary Computational Science Program in the Center for Computational Sciences, University of Tsukuba.

1. J. R. Shen, The structure of photosystem II and the mechanism of water oxidation in photosynthesis. *Annu. Rev. Plant Biol.* **66**, 23–48 (2015).
2. H. Michel, J. Deisenhofer, Relevance of the photosynthetic reaction center from purple bacteria to the structure of photosystem II. *Biochemistry* **27**, 1–7 (1988).
3. W. Zinth, J. Wachtveitl, The first picoseconds in bacterial photosynthesis—ultrafast electron transfer for the efficient conversion of light energy. *ChemPhysChem* **6**, 871–880 (2005).
4. S. Vasil'ev, P. Orth, A. Zouni, T. G. Owens, D. Bruce, Excited-state dynamics in photosystem II: Insights from the x-ray crystal structure. *Proc. Natl. Acad. Sci. U.S.A.* **98**, 8602–8607 (2001).
5. S. Vasil'ev, D. Bruce, A protein dynamics study of photosystem II: The effects of protein conformation on reaction center function. *Biophys. J.* **90**, 3062–3073 (2006).
6. V. V. Klimov, S. I. Allakhverdiev, S. Demeter, A. A. Krasnovskii, Photoreduction of pheophytin in the photosystem 2 of chloroplasts with respect to the redox potential of the medium. *Dokl. Akad. Nauk SSSR* **249**, 227–230 (1979).
7. A. W. Rutherford, J. E. Mullet, A. R. Crofts, Measurement of the midpoint potential of the pheophytin acceptor of photosystem II. *FEBS Lett.* **123**, 235–237 (1981).
8. K. Saito *et al*., Distribution of the cationic state over the chlorophyll pair of the photosystem II reaction center. *J. Am. Chem. Soc.* **133**, 14379–14388 (2011).
9. F. Rappaport, M. Guergova-Kuras, P. J. Nixon, B. A. Diner, J. Lavergne, Kinetics and pathways of charge recombination in photosystem II. *Biochemistry* **41**, 8518–8527 (2002).
10. J. C. Williams *et al*., Effects of mutations near the bacteriochlorophylls in reaction centers from *Rhodobacter sphaeroides*. *Biochemistry* **31**, 11029–11037 (1992).
11. M. Mandal, K. Kawashima, K. Saito, H. Ishikita, Redox potential of the oxygen-evolving complex in the electron transfer cascade of photosystem II. *J. Phys. Chem. Lett.* **11**, 249–255 (2020).
12. M. R. Gunner, A. Nicholls, B. Honig, Electrostatic potentials in *Rhodopseudomonas viridis* reaction centers: Implications for the driving force and directionality of electron transfer. *J. Phys. Chem.* **100**, 4277–4291 (1996).
13. D. J. Lockhart, S. G. Boxer, Stark effect spectroscopy of *Rhodobacter sphaeroides* and *Rhodopseudomonas viridis* reaction centers. *Proc. Natl. Acad. Sci. U.S.A.* **85**, 107–111 (1988).
14. T. Cardona, A. Sedoud, N. Cox, A. W. Rutherford, Charge separation in photosystem II: A comparative and evolutionary overview. *Biochim. Biophys. Acta* **1817**, 26–43 (2012).
15. L. M. McDowell, C. Kirmaier, D. Holten, Charge transfer and charge resonance states of the primary electron donor in wild-type and mutant bacterial reaction centers. *Biochim. Biophys. Acta* **1020**, 239–246 (1990).
16. L. M. McDowell, D. Gaul, C. Kirmaier, D. Holten, C. C. Schenck, Investigation into the source of electron transfer asymmetry in bacterial reaction centers. *Biochemistry* **30**, 8315–8322 (1991).
17. B. A. Heller, D. Holten, C. Kirmaier, Effects of Asp residues near the L-side pigments in bacterial reaction centers. *Biochemistry* **35**, 15418–15427 (1996).
18. M. A. Harris *et al*., Protein influence on charge-asymmetry of the primary donor in photosynthetic bacterial reaction centers containing a heterodimer: Effects on photophysical properties and electron transfer. *J. Phys. Chem. B* **117**, 4028–4041 (2013).
19. K. Kawashima, H. Ishikita, Energetic insights into two electron transfer pathways in light-driven energy-converting enzymes. *Chem. Sci.* **9**, 4083–4092 (2018).
20. U. Finkele, C. Lauterwasser, W. Zinth, K. A. Gray, D. Oesterhelt, Role of tyrosine M210 in the initial charge separation of reaction centers of *Rhodobacter sphaeroides*. *Biochemistry* **29**, 8517–8521 (1990).
21. H. L. Axelrod *et al*., X-ray structure determination of the cytochrome c_2: Reaction center electron transfer complex from *Rhodobacter sphaeroides*. *J. Mol. Biol.* **319**, 501–515 (2002).
22. A. W. Rutherford, "Photosystem II, the oxygen evolving photosystem" in *Light-Energy Transduction in Photosynthesis: Higher Plant and Bacterial Models*, S. Stevens, D. A. Bryant, Eds. (American Society of Plant Physiology, Rockville, MD, 1988), pp. 163–177.
23. V. I. Prokhorenko, A. R. Holzwarth, Primary process and structure of the photosystem II reaction center: A photon echo study. *J. Phys. Chem. B* **104**, 11563–11578 (2000).
24. J. P. Dekker, R. van Grondelle, Primary charge separation in Photosystem II. *Photosynth. Res.* **63**, 195–208 (2000).
25. K. Saito, T. Suzuki, H. Ishikita, Absorption-energy calculations of chlorophyll *a* and *b* with an explicit solvent model. *J. Photochem. Photobiol. Chem.* **358**, 422–431 (2018).
26. K. M. Barkigia, L. Chantranupong, K. M. Smith, J. Fajer, Structural and theoretical models of photosynthetic chromophores. Implications for redox, light-absorption properties and vectorial electron flow. *J. Am. Chem. Soc.* **110**, 7566–7567 (1988).
27. K. Saito *et al*., Deformation of chlorin rings in the Photosystem II crystal structure. *Biochemistry* **51**, 4290–4299 (2012).
28. H. Tamura, Diabatization for time-dependent density functional theory: Exciton transfers and related conical intersections. *J. Phys. Chem. A* **120**, 9341–9347 (2016).
29. W. W. Parson, Z.-T. Chu, A. Warshel, Electrostatic control of charge separation in bacterial photosynthesis. *Biochim. Biophys. Acta* **1017**, 251–272 (1990).
30. M. Sugiura *et al*., The D1-173 amino acid is a structural determinant of the critical interaction between D1-Tyr161 (TyrZ) and D1-His190 in Photosystem II. *Biochim. Biophys. Acta* **1837**, 1922–1931 (2014).
31. I. Rivalta *et al*., Structural-functional role of chloride in photosystem II. *Biochemistry* **50**, 6312–6315 (2011).
32. K. Saito, A. W. Rutherford, H. Ishikita, Mechanism of tyrosine D oxidation in photosystem II. *Proc. Natl. Acad. Sci. U.S.A.* **110**, 7690–7695 (2013).
33. K. Saito, N. Sakashita, H. Ishikita, Energetics of the proton transfer pathway for tyrosine D in photosystem II. *Aust. J. Chem.* **69**, 991–998 (2016).
34. P. Manna, R. LoBrutto, C. Eijckelhoff, J. P. Dekker, W. Vermaas, Role of Arg180 of the D2 protein in photosystem II structure and function. *Eur. J. Biochem.* **251**, 142–154 (1998).
35. S. E. J. Rigby, J. H. A. Nugent, P. J. O'Malley, ENDOR and special triple resonance studies of chlorophyll cation radicals in photosystem 2. *Biochemistry* **33**, 10043–10050 (1994).
36. B. A. Diner *et al*., Site-directed mutations at D1-His198 and D2-His197 of photosystem II in *Synechocystis* PCC 6803: Sites of primary charge separation and cation and triplet stabilization. *Biochemistry* **40**, 9265–9281 (2001).
37. M. Sugiura *et al*., Site-directed mutagenesis of *Thermosynechococcus elongatus* photosystem II: The O_2-evolving enzyme lacking the redox-active tyrosine D. *Biochemistry* **43**, 13549–13563 (2004).
38. Y. Kato, R. Nagao, T. Noguchi, Redox potential of the terminal quinone electron acceptor Q_B in photosystem II reveals the mechanism of electron transfer regulation. *Proc. Natl. Acad. Sci. U.S.A.* **113**, 620–625 (2016).
39. M. Saggu, S. D. Fried, S. G. Boxer, Local and global electric field asymmetry in photosynthetic reaction centers. *J. Phys. Chem. B* **123**, 1527–1536 (2019).
40. K. N. Ferreira, T. M. Iverson, K. Maghlaoui, J. Barber, S. Iwata, Architecture of the photosynthetic oxygen-evolving center. *Science* **303**, 1831–1838 (2004).
41. H. Ishikita, W. Saenger, B. Loll, J. Biesiadka, E.-W. Knapp, Energetics of a possible proton exit pathway for water oxidation in photosystem II. *Biochemistry* **45**, 2063–2071 (2006).
42. R. J. Debus, Evidence from FTIR difference spectroscopy that D1-Asp61 influences the water reactions of the oxygen-evolving Mn_4CaO_5 cluster of photosystem II. *Biochemistry* **53**, 2941–2955 (2014).
43. K. Kawashima, T. Takaoka, H. Kimura, K. Saito, H. Ishikita, O_2 evolution and recovery of the water-oxidizing enzyme. *Nat. Commun.* **9**, 1247 (2018).
44. R. Pokhrel, R. J. Service, R. J. Debus, G. W. Brudvig, Mutation of lysine 317 in the D2 subunit of photosystem II alters chloride binding and proton transport. *Biochemistry* **52**, 4758–4773 (2013).
45. A. Boussac, A. W. Rutherford, The origin of the split S_3 EPR signal in Ca^{2+}-depleted photosystem II: Histidine versus tyrosine. *Biochemistry* **31**, 7441–7445 (1992).
46. H. Wincencjusz, H. J. van Gorkom, C. F. Yocum, The photosynthetic oxygen evolving complex requires chloride for its redox state $S_2 \rightarrow S_3$ and $S_3 \rightarrow S_0$ transitions but not for $S_0 \rightarrow S_1$ or $S_1 \rightarrow S_2$ transitions. *Biochemistry* **36**, 3663–3670 (1997).
47. A. W. Rutherford, P. Faller, Photosystem II: Evolutionary perspectives. *Philos. Trans. R. Soc. Lond. B Biol. Sci.* **358**, 245–253 (2003).
48. T. Cardona, J. W. Murray, A. W. Rutherford, Origin and evolution of water oxidation before the last common ancestor of the cyanobacteria. *Mol. Biol. Evol.* **32**, 1310–1328 (2015).
49. K. Saito, J.-R. Shen, T. Ishida, H. Ishikita, Short hydrogen bond between redox-active tyrosine Y_Z and D1-His190 in the photosystem II crystal structure. *Biochemistry* **50**, 9836–9844 (2011).
50. N. Sakashita, H. C. Watanabe, T. Ikeda, K. Saito, H. Ishikita, Origins of water molecules in the photosystem II crystal structure. *Biochemistry* **56**, 3049–3057 (2017).

51. R. J. Debus, FTIR studies of metal ligands, networks of hydrogen bonds, and water molecules near the active site Mn_4CaO_5 cluster in Photosystem II. *Biochim. Biophys. Acta* **1847**, 19–34 (2015).
52. Y. Umena, K. Kawakami, J.-R. Shen, N. Kamiya, Crystal structure of oxygen-evolving photosystem II at a resolution of 1.9 Å. *Nature* **473**, 55–60 (2011).
53. P. Cieplak, J. Caldwell, P. Kollman, Molecular mechanical models for organic and biological systems going beyond the atom centered two body additive approximation: Aqueous solution free energies of methanol and *N*-methyl acetamide, nucleic acid base, and amide hydrogen bonding and chloroform/water partition coefficients of the nucleic acid bases. *J. Comput. Chem.* **22**, 1048–1057 (2001).
54. S. Nakamura, T. Noguchi, Infrared determination of the protonation state of a key histidine residue in the photosynthetic water oxidizing center. *J. Am. Chem. Soc.* **139**, 9364–9375 (2017).
55. C. I. Bayly, P. Cieplak, W. D. Cornell, P. A. Kollman, A well-behaved electrostatic potential based method using charge restraints for deriving atomic charges: The RESP model. *J. Phys. Chem.* **97**, 10269–10280 (1993).
56. N. M. Thellamurege *et al*., QuanPol: A full spectrum and seamless QM/MM program. *J. Comput. Chem.* **34**, 2816–2833 (2013).
57. M. W. Schmidt *et al*., General atomic and molecular electronic-structure system. *J. Comput. Chem.* **14**, 1347–1363 (1993).
58. S. Grimme, Semiempirical GGA-type density functional constructed with a long-range dispersion correction. *J. Comput. Chem.* **27**, 1787–1799 (2006).
59. T. Yanai, D. P. Tew, N. C. Handy, A new hybrid exchange-correlation functional using the Coulomb-attenuating method (CAM-B3LYP). *Chem. Phys. Lett.* **393**, 51–57 (2004).
60. H. Tamura *et al*., Theoretical analysis on the optoelectronic properties of single crystals of thiophene-furan-phenylene co-oligomers: Efficient photoluminescence due to molecular bending. *J. Phys. Chem. C* **117**, 8072–8078 (2013).
61. S. Nakamura, T. Noguchi, Infrared detection of a proton released from tyrosine Y_D to the bulk upon its photo-oxidation in photosystem II. *Biochemistry* **54**, 5045–5053 (2015).
62. F. M. Ho, "Substrate and product channels in photosystem II" in *Molecular Solar Fuels*, T. J. Wydrzynski, W. Hillier, Eds. (RSC Energy and Environment Series, RSC Publishing, 2012), pp. 208–248.
63. S. Iwata, J. Barber, Structure of photosystem II and molecular architecture of the oxygen-evolving centre. *Curr. Opin. Struct. Biol.* **14**, 447–453 (2004).